ingegneria sismica
International Journal of Earthquake Engineering
Anno XLIII - Num. 2 - 2026

Strategies to suppress the formation of polycyclic aromatic hydrocarbons during food processing and their impact on product flavor quality

Weize Mao[1,*]

[1] Xinxiang Institute of Engineering, Xinxiang, Henan, 453000, China

SUMMARY: *During thermal processing, the generation of polycyclic aromatic hydrocarbons (pahs) is strongly coupled with temperature fluctuations, lipid oxidation, smoke deposition, and volatile release, making it difficult to optimize risk mitigation and flavor retention simultaneously. In this paper, we construct a data-driven food processing control evaluation framework that incorporates multi-source sensing, feature fusion, and process optimization. The risk identification model and flavor quality evaluation model of pahs were established by synchronizing spectral signal, gas sensitivity response, temperature distribution and product color characteristics, and the roasting temperature, heating time, air flow and surface moisture were multi-objective optimized. Experimental results show that the proposed framework achieves 97.8% risk identification accuracy, 0.986 AUC and 94.3% flavor quality classification accuracy. After optimization, the total content of polycyclic aromatic hydrocarbons was reduced by 31.6%, the retention rate of key ideal volatiles was 89.4%, and the sensory acceptance was improved from 8.1 to 8.8. This framework provides a more stable and computable way to intelligently suppress the generation of harmful substances while maintaining product flavor consistency under uncertain processing conditions.*

KEYWORDS: *Polycyclic aromatic hydrocarbons; Multi-source sensing; Data-driven optimization; Flavor quality assessment*

1 Introduction

Food thermal processing can not only endow products with color, texture and flavor, but also induce the formation of polycyclic aromatic hydrocarbons due to lipid cracking, protein thermal degradation and flue gas deposition. The formation level of polycyclic aromatic hydrocarbons is closely related to heating temperature, processing time, surface oil content, moisture content and local airflow conditions. Dutta et al. systematically analyzed the formation rules and avoidance paths of pahs in meat and fish under high-risk cooking methods, indicating that the selection of front-end processing methods itself is an important variable for pollutant control [1]. Wei et al. proposed a machine learning quantitative method based on synchronous fluorescence spectroscopy to realize the rapid synchronous identification of pahs in edible oil, indicating that intelligent modeling can improve the efficiency of pollutant detection in complex food systems [2]. It can be seen that in food processing scenarios, the combination of hazard control with digital perception, pattern recognition and process optimization has become an important direction from empirical regulation to fine control.

*MWZ_studio@163.com
https://doi.org/10.65102/is2026555
Published: 30 April, 2026

Hao et al. used fluorescence hyperspectral technology to quantitatively analyze polycyclic aromatic hydrocarbons in Tan sheep, and proved the effectiveness of joint characterization of spatial and spectral information [3]. Zhang et al. constructed a machine learning prediction model for the bioavailability of maternal and substituted pahs in food, which improved the quantitative accuracy of risk assessment [4]. Patil et al. established a prediction framework around changes in total polar components of frying oil, revealing the mapping relationship between oil deterioration indicators and processing time, and providing a transferable idea for modeling the formation process of hazards [5]. Bose et al. used electronic nose technology combined with machine learning classifier to evaluate hexanal level in potato chips, expanding the technical path for rapid identification of processing odors [6]. Jia et al. proposed a fusion detection method of near-infrared and electronic nose, and improved the stability of adulterated meat identification through data fusion, indicating that multi-source feature collaboration is conducive to enhancing the robustness of the model [7]. Aqeel et al. applied hyperspectral imaging and machine learning to oil adulteration identification, and verified the practical value of band selection, feature compression and classification learning in complex quality identification [8]. Ji et al. summarized the application progress of machine learning in food flavor prediction and regulation, and pointed out that the research on flavor formation was shifting from empirical judgment to data-driven association learning [9]. Cai et al. summarized the characteristic flavor determination strategy from the perspective of the collaboration of flavor omics and machine learning, and provided a clear method framework for complex quality analysis [10].

Table 1: Summary of related work

Method Direction	Main Research Object	Computer Technology Features	Existing Limitations
Spectral and Hyperspectral Recognition	Polycyclic aromatic hydrocarbons, oil quality	Feature extraction, band optimization, classification and regression	Insufficient adaptability to dynamic processing conditions
Electronic Nose and Sensor Arrays	Odor, volatile compounds, oxidation state	Pattern recognition, multi-source fusion	Difficult to directly characterize pollutant formation processes
Flavoromics Modeling	Aroma types, sensory attributes	Machine learning, deep learning, interpretable analysis	Insufficient coordination between safety and flavor optimization
Process Parameter Optimization	Temperature, time, moisture content, airflow	Multi-objective optimization, process modeling	Online closed-loop control capability still needs to be strengthened

Gharibzahedi et al. reviewed the application of electronic sensor technology in tea quality monitoring, indicating that sensor arrays can quickly characterize complex flavor and quality states [11]. Zhang et al. summarized the research progress of near-infrared spectroscopy machine learning and proved the versatility of nondestructive testing and rapid modeling in food quality analysis [12]. Lee et al. realized sweetener representation by molecular sensing representation learning, which promoted flavor perception from experience classification to representation learning [13]. Bo et al. established prediction models of bitter agents and

sweeteners based on artificial neural networks, which reflected the computable mapping relationship between structural information and perception results [14]. Yang et al. proposed a multi-layer sweetness prediction method to enhance the system representation ability of sensory intensity [15]. Maroni et al. used explainable machine learning to classify sweeteners and bitters, improving the interpretation clarity between model output and perception results [16]. Cardoso Schwindt et al. discussed the applicability of QSOR modeling and machine learning in wine aroma prediction, and proved that chemical characteristics can be quantitatively correlated with flavor perception [17]. Qiu et al. carried out yogurt aroma type classification research based on flavor omics, and improved the accuracy of complex aroma spectrum recognition [18]. Sun et al. combined hyperspectral imaging and machine learning to identify the odor of farmed salmon trout, indicating that the joint modeling of spatial information and chemical information is suitable for handling the task of flavor defect detection [19]. Shen et al. combined deep learning, stoichiometry and sensory evaluation to predict the volatile component content and baking mode of mutton skewers, reflecting the integration trend of processing mode identification and flavor result prediction [20].

Based on the existing research, the relevant achievements have covered the detection of pahs, identification of oil deterioration, volatile monitoring and flavor classification, etc. However, most of the work is still focused on single endpoint discrimination, and the dynamic coupling between the generation process of pahs, the flavor preservation target and the processing parameters is not well described. There is a lack of an integrated framework for risk identification, parameter optimization and process regulation in actual food processing scenarios. Based on this, this paper focuses on the suppression of pahs generation and the impact assessment of product flavor quality in food processing. From the perspective of food safety control and intelligent manufacturing, the relationship between pahs generation and flavor quality evolution is analyzed, and on this basis, an intelligent generation risk identification method based on multi-source perception data fusion is constructed. Furthermore, the processing parameter optimization method was designed for the collaborative goal of PAH suppression and flavor preservation, and finally the process control strategy embedded in the data-driven model was formed. This paper is expected to complete the quantitative evaluation from the aspects of recognition accuracy, model operation efficiency, reduction of pahs, retention rate of key volatiles and change of sensory acceptance, so as to provide computational, executable and verifiable technical support for intelligent safety control and stable flavor retention in food processing scenarios.

2 Methods and materials

2.1 Mechanism analysis of polycyclic aromatic hydrocarbons generation and flavor quality evolution during food processing

Besides the formation of color, organization and scorching characteristics, food thermal processing can also trigger parallel processes such as lipid cleavage, protein thermal degradation, glycosylation rearrangement and smoke back adhesion. Pahs precursors and key volatile precursors evolve synchronously in the same heating window, so this process cannot be explained by only a single temperature index. In order to provide the mechanism support for the subsequent identification model and parameter optimization strategy, this section establishes the calculation and analysis framework around heat transfer, oxygen diffusion, surface carbonization, volatile substance migration and color response, and converts the temperature field, air flow field, surface moisture content, lipid load and spectral response into state variables that can be read by the algorithm.

As shown in Fig. 1, the food sample forms a hierarchical evolution path between the heated surface, the boundary gas layer, and the internal tissue. Dehydration and contraction occur in the outer layer, followed by lipid fragmentation and release of aromatic intermediates at high temperatures. Maillard reactions and carbonyl rearrangements occur continuously in the middle layer, while the inner region maintains high water content and forms a delayed buffer against heat diffusion. The infrared temperature distribution, electronic nose response, surface color characteristics and spectral reflection signals are collected synchronously at the sensing end, and the state reconstruction is completed at the computing end according to these signals, so that the generation trend of pahs and the flavor release trajectory can be jointly characterized.

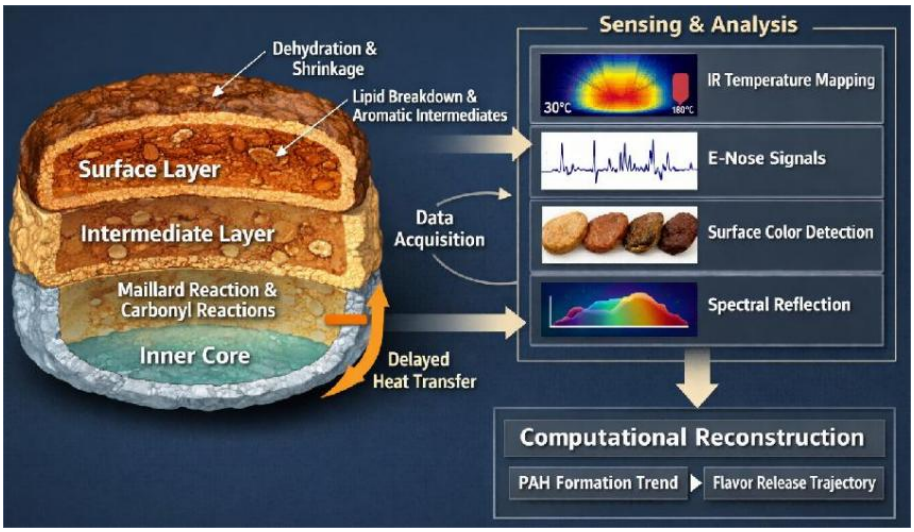

Figure 1: Diagram of the coupling mechanism between PAH precursor generation and flavor precursor migration under thermal processing conditions

In order to uniformly write the thermal reaction intensity, oxidation accumulation, surface deposition and local water loss effect into the state space mapping process, the following risk-driven function can be constructed.

$$G_a = \int_0^{\tau} \exp(\kappa_1 \Theta(t)) \; [\Omega(t)]^{\kappa_2} \; (1 + \Lambda(t)) \, \Gamma(t) \, dt \tag{1}$$

In equation (1), G_a represents the driving force of PAH generation, $\Theta(t)$ represents the surface thermal intensity trajectory, $\Omega(t)$ represents the lipid oxidation activity, $\Lambda(t)$ represents the flue gas backattachment coefficient, $\Gamma(t)$ represents the water loss amplification term, κ_1 and κ_2 are sensitive parameters, and τ is the processing duration. Thermal, oxidation and deposition effects are compressed into continuous risk quantities, which is convenient for time series comparison and threshold discrimination of the model.

In the actual processing, the flavor does not continue to enhance with the heat input. Some aldehydes, ketones and sulfur-containing volatiles were released obviously under moderate heat load, and when the surface carbonization continued to deepen, the original aroma components began to decay, and some esters also escaped in advance due to local wind speed enhancement. Therefore, the flavor evolution needs to consider the generation, retention and loss channels at the same time.

In order to simultaneously describe the coupling relationship between volatile generation contribution, retention capacity, thermal attenuation and dissipation loss, the following

comprehensive flavor response potential function can be defined.

$$F_b = \sum_{m=1}^{M} \frac{\Psi_m \Upsilon_m(\xi_m)}{1 + \exp(\rho_m \Delta_m)} - \int_0^{\tau} X(t)\, \Phi(t)\, dt \tag{2}$$

In equation (2), F_b represents the integrated flavor response value, Ψ_m represents the sensory weight of key volatilates, $\Upsilon_m(\xi_m)$ represents the generative contribution obtained from the precursor conversion efficiency ξ_m, ρ_m represents the thermal attenuation coefficient, Δ_m represents the thermal exposure bias, $X(t)$ represents the airflow peel strength, and $\Phi(t)$ represents the pore dissipation term. This formula puts flavor enhancement and flavor loss in the same frame, which can explain the difference of sensory results under the same reduction amplitude.

As shown in Fig. 2, when the continuous state is obtained at the computing end, the surface layer, boundary layer and inner layer of the sample can be divided into three associated nodes, and the information of heat flux, oxygen diffusion and precursor transformation can be updated in time slices. In the figure, the left is the physical perception link, the middle is the state reconstruction link, and the right is the quality output link. The structure suggests that both PAH generation and flavor variation result from the associated accumulation of multi-source states.

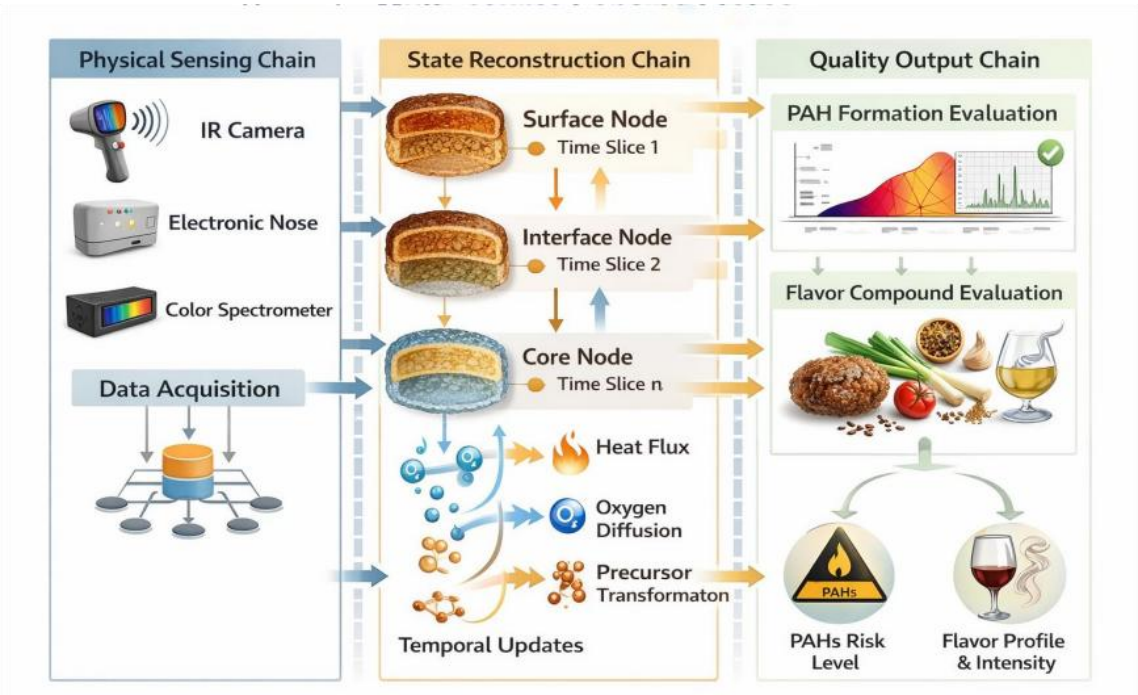

Figure 2: Computational graph of risk-flavor joint evolution driven by multi-source sensing states

In order to describe the energy propagation, precursor exchange speed and state inheritance relationship between different spatial layers of the sample, the following calculation expressions for updating hierarchical associated nodes can be established.

$$X_i^{(n+1)} = \sigma\left(\Pi_i X_i^{(n)} + \sum_{j \in \mathcal{N}_i} \varpi_{ij} B_{ij} X_j^{(n)} + \eta_i U_i^{(n)} \right) \tag{3}$$

In Equation (3), $X_i^{(n)}$ represents the state vector of the i layer node at the n time slice, Π_i represents the intra-layer self-updating matrix, ϖ_{ij} represents the transfer weight, B_{ij} represents the cross-layer coupling transformation matrix, $\mathcal{N}_i$ represents the neighborhood set, η_i represents the exogenous injection coefficient,$U_i^{(n)}$ represents the sensing input, and σ is the nonlinear activation operator. This formula embodies the idea of state propagation, and can translate local changes into iterative digital representations.

In order to obtain the total result of evolution decision that takes into account the safety constraint, flavor threshold, color consistency and odor penalty, the overall collaborative evaluation discriminant can be further constructed as follows.

$$C_\zeta = \mu_1 \tanh(H_\zeta) + \mu_2 \ln(1 + K_\zeta) + \mu_3 \exp\left(-|Y_p - Y_q|\right) - \mu_4 N_\zeta \tag{4}$$

In Formula (4), C_ζ represents the collaborative evaluation value of the processing state, μ_1 to μ_4 are the weight coefficients, H_ζ represents the safety margin mapping quantity, K_ζ represents the flavor retention mapping quantity, Y_p represents the real-time color representation quantity, Y_q represents the target color reference quantity, and N_ζ represents the odor offset penalty term. The formula is used to connect mechanism analysis and process control, so that the system retains acceptable flavor profile and appearance consistency when suppressing the generation of pahs, and forms the starting point for subsequent online decision calculation, and supports subsequent risk identification and modeling.

Based on the above analysis, it can be seen that the formation of pahs in food thermal processing is not the result of a single thermal reaction, but a coupled evolution process formed by surface carbonization, lipid cracking, oxygen diffusion, smoke deposition and volatile migration. The change of flavor quality does not occur independently, and its formation intensity, release rhythm and loss rate are always synchronously restricted by local thermal state and tissue mass transfer conditions. After state variable extraction, hierarchical node representation and collaborative evaluation representation, the safety information, flavor information and appearance information in the process have been uniformly translated into computable structured inputs.

2.2 Intelligent identification method of pahs generation risk based on multi-source sensing data fusion

The state change of the thermal processing site does not depend on a single signal presentation. The infrared thermal image records the surface heat distribution, the gas sensitive array reflects the volatile response, the color image represents the Browning degree, and the reflection spectrum corresponds to the chemical composition change. Different information sources have obvious differences in sampling frequency, dimension range and response delay. If the input is directly spliced, the model is easy to mistake local peaks for global risk evidence. Based on this feature, in this study, multi-source signals are mapped into time-aligned processing event segments, and a deep fusion recognition structure is established on this basis, so that the generation trend of pahs can be continuously discriminated during the processing process.

As shown in Fig. 3, the identification method consists of a data access layer, a modal coding layer, a cross-source fusion layer, and a risk output layer. The data access layer is responsible for receiving the infrared frame, gas sensing sequence, color matrix and spectral vector after synchronization slicing. The modal coding layer extracts thermal gradient texture, volatile fluctuation features, color statistical information and spectral compression representation respectively. The cross-source fusion layer completes the gating weighting and joint representation construction. The risk output layer gives the low, medium and high risk probabilities of pahs. The structure is not simply superimposed sensors, but transcribe the information from different sources into a unified event representation, and then reconstruct the risk evidence chain by the fusion network.

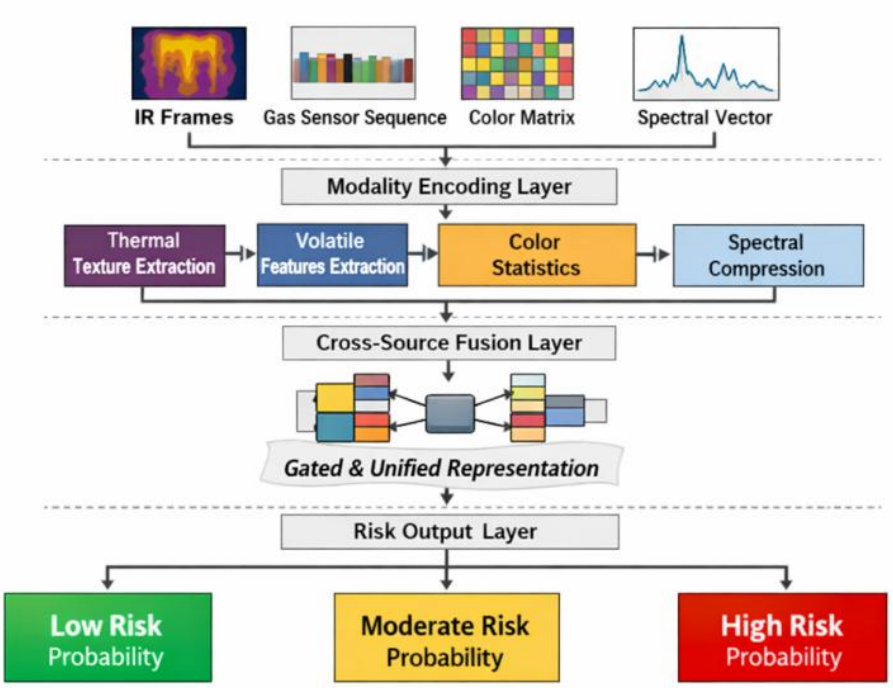

Figure 3: Structural diagram of PAH generation risk identification for multi-source sensing data fusion

In order to make the thermography, gas sensing, color and spectral sequences form comparable inputs on the same time slice and retain processing event boundary information, the following alignment expression can be written.

$$M_s = \mathrm{Concat}\left(\frac{A_s - a_0}{a_1}, \frac{B_s - b_0}{b_1}, \frac{C_s - c_0}{c_1}, \frac{D_s - d_0}{d_1}\right) \tag{5}$$

In Formula (5), M_s represents the unified input vector of the s processing event, A_s, B_s, C_s and D_s represent the infrared thermal image feature, gas sensitive response feature, color statistical feature and spectral compression feature respectively, a_0 to d_0 are the reference centers of each mode, and a_1 to d_1 are the scale factors. This formula is used to complete the time alignment and dimension normalization of multi-source input.

In order to adaptively allocate the contribution ratio of each mode according to the current stability degree and effective information density, and reduce the bias influence of abnormal fluctuations on the identification results, the reliability expression can be defined as follows.

$$R_s = \mathrm{Softmax}(PM_s + q) \tag{6}$$

In equation (6), R_s represents the modal reliability vector of the s event segment, P is the weight mapping matrix, and q is the bias vector. The formula uses Softmax to compress the feature credibility of different sources into comparable weights, which are used for dynamic redistribution in the subsequent fusion stage.

In order to preserve both local response strength and nonlinear structure information during the encoding process, and enhance the ability of the model to distinguish high-risk processing segments, the following gated encoding formula can be established.

$$K_s = \left[\frac{1}{2}(UM_s)\left(1 + \mathrm{erf}\left(\frac{UM_s}{\sqrt{2}}\right)\right)\right] \circ \frac{1}{1 + \exp(-VM_s)} \tag{7}$$

In Formula (7), K_s represents the output feature of the s processing event segment after gated coding, M_s represents the unified input vector of the event segment, U and V represent two sets of trainable feature mapping matrices, $\circ$ represents element-wise multiplication, and $\mathrm{erf}(\cdot)$ is the error function used to construct a continuous and smooth nonlinear response term. $\exp(\cdot)$ is the natural exponential function used to generate gating weights that range from 0 to 1. In the formula, the left bracket term corresponds to the continuous nonlinear mapping result of the input feature, and the right fractional term corresponds to the gated inhibition and enhancement result. The coupling of the two parts can retain the effective thermal processing information while weakening the interference of redundant fluctuations on the recognition results, thus enhancing the model's ability to characterize the risk pattern of PAH generation and weak differential flavor signals.

In order to strengthen the association relationship between effective evidence in the cross-source fusion stage and suppress the interference of background noise and redundant texture on risk discrimination, the attention mapping formula can be written as follows.

$$J_s = \mathrm{Softmax}\left(\frac{K_s L_s^{\top}}{\sqrt{\ell}}\right) N_s \tag{8}$$

In Equation (8), J_s represents the fused joint representation, L_s is the key vector matrix, N_s is the value vector matrix, and ℓ is the scaling constant. This formula realizes cross-source attention focusing through correlation normalization, so that thermal anomalies, volatilization offsets and color changes can form linkage in the same representation space.

In order to map the joint representation into a comparable risk probability output, while taking into account the class boundary clarity and the overall convergence stability in the training phase, the recognition objective function can be defined as follows.

$$\mathcal{L}_{\mathrm{risk}} = -\sum_{h=1}^{H} t_{s,h} \log \hat{z}_{s,h} + \beta_0 \|O\|_2^2 + \beta_1 (1 - AUC_s) \tag{9}$$

In Equation (9), $\mathcal{L}_{\mathrm{risk}}$ represents the total risk identification loss, $t_{s,h}$ is the true label of the s sample on the h class, $\hat{z}_{s,h}$ is the predicted probability, O is the classification head parameter matrix, and β_0 and β_1 are the regular weights. In addition to the cross-entropy constraint, parameter smoothing and AUC correction are added to make the identification of high-risk samples more stable.

When the model is trained, the input samples enter the network according to the batch event stream. The stable local structure is learned by the low-level encoder, and then the update range of the fusion layer and the classification head is gradually released, so that

different modalities form effective collaboration in the middle and late stages. The validation phase simultaneously monitors precision, recall, and AUC to avoid the model relying on only a single statistical metric.

2.3 Processing parameter optimization method for the synergy goal of PAH suppression and flavor preservation

After the risk identification method is constructed, the processing parameter optimization method for the collaborative goal of PAH suppression and flavor preservation can be further designed. Baking temperature, heating time, air intensity and surface moisture content in food hot processing will act on surface carbonization, flue gas back attachment, volatile release and color formation. If the adjustment is carried out only around the reduction of pollutants, excessive loss of key aroma components often occurs. If only aroma retention is emphasized, local overheating is easy to push up the level of pahs. Therefore, in this study, the safety index, flavor index, appearance index and process execution boundary are simultaneously written into the unified search space, and the data-driven surrogate model is used to quickly solve the problem, so that the optimization process is computable and executable.

Before the machining parameters enter the optimization layer, the system completes the parameter coding. The baking temperature is mapped as a continuous control quantity, the heating time is segmented according to the window of seconds, the air flow intensity is converted into a standardized variable according to the gear of the equipment, and the surface moisture content is formed into an interval value through the process of spray water filling and standing absorption. Each set of candidate parameters is jointly evaluated by the risk identification model and the flavor evaluation branch of the previous section to obtain risk probability, retention of key volatiles, integrated color difference shift, and sensory score prediction values. In this way, the optimization process no longer relies on group-by-group trials, but is based on model-surrogate evaluations.

As shown in Fig. 4, the collaborative optimization structure consists of a parameter encoding unit, an agent evaluation unit, a candidate update unit, and an optimal solution output unit. The parameter coding unit is responsible for generating the process combination to be searched. The proxy assessment unit computes pahs risk, flavor retention, color deviation and sensory scores in parallel. The candidate update unit adjusted the next search direction according to the change of the objective function. The optimal solution output unit gives the final set of parameters that satisfy the synergy constraints. The process adopts a rolling update mode, so that different batches of samples can obtain comparable optimal processes under a unified criterion.

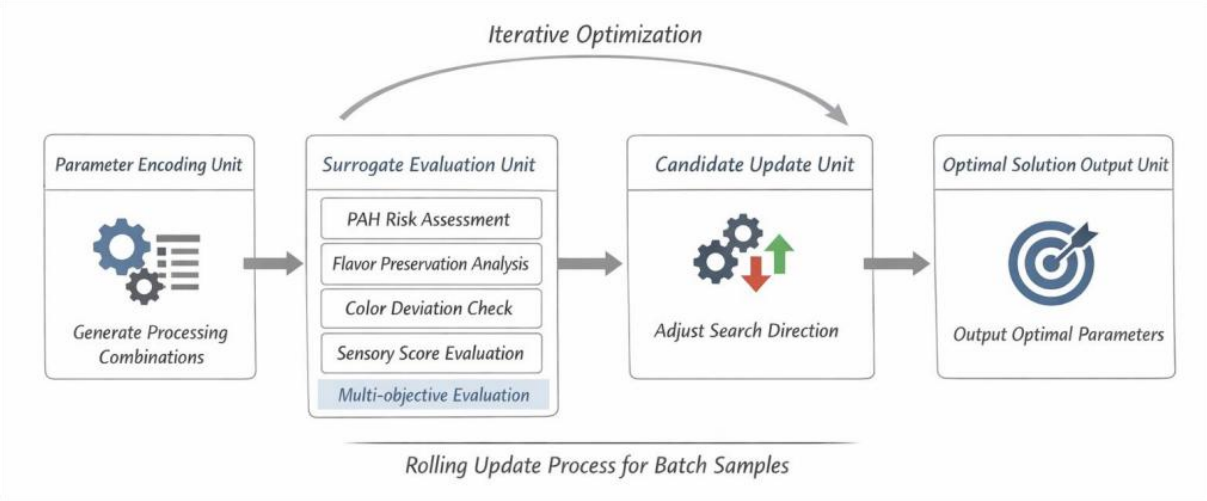

Figure 4: Flowchart of processing parameter optimization for the synergy objective of PAH suppression and flavor preservation

In order to compress the security risk, volatile retention, color deviation and sensory prediction results into a unified search objective and maintain a comparable scale between each index, it can be expressed as the following equation.

$$\mathfrak{J}_r = \alpha_1 \hat{p}_r - \alpha_2 \hat{f}_r + \alpha_3 \hat{c}_r - \alpha_4 \hat{s}_r \tag{10}$$

In Formula (10), $\mathfrak{J}_r$ represents the comprehensive target value of the r round of search, $\hat{p}_r$ is the risk prediction of pahs, $\hat{f}_r$ is the retention prediction of key volatiles, $\hat{c}_r$ is the comprehensive color deviation, $\hat{s}_r$ is the sensory score prediction, and α_1 to α_4 are the target weights. The formula puts safety and quality into the same evaluation framework, which is convenient for subsequent search and comparison.

In order to make the candidate parameters not only maintain the exploration ability but also gradually approach the current better region in the optimization process, the parameter update relationship can be written in the following form.

$$W_{r+1} = W_r + \alpha_5 u_r + \alpha_6 (W_r^\star - W_r) \tag{11}$$

In Equation (11), W_r represents the parameter vector in round r, $W_r^\star$ represents the current optimal candidate parameter, u_r represents the perturbation direction vector, and α_5 and α_6 represent the exploration step and the contraction step, respectively. This formula takes into account both global search and local approximation, which is conducive to improving convergence efficiency.

In order to ensure that the candidate process not only dominates the numerical objective, but also satisfies the equipment execution boundary and product processing feasibility constraints, the feasibility criteria can be further defined as follows.

$$\mathfrak{P}_r = \mathbb{I}(g_{1,r} \le \bar{g}_1)\mathbb{I}(g_{2,r} \le \bar{g}_2)\mathbb{I}\left(g_{3,r} \in [\underline{g}_3, \bar{g}_3]\right) \tag{12}$$

In Equation (12), $\mathfrak{P}_r$ represents the feasibility mark of the candidate solution in round r, $g_{1,r}$ represent the temperature change gradient, $g_{2,r}$ represent the airflow switching amplitude, $g_{3,r}$ represent the water replantation frequency, and $\bar{g}_1$, $\bar{g}_2$, $\underline{g}_3$ and $\bar{g}_3$ are the corresponding boundaries. This formula is used to filter out candidate parameters that are

mathematically feasible but difficult for the device to perform stably.

In order to screen out the final process combination after multiple rounds of search, which takes into account the objective value, execution stability and batch adaptability, the following synthesis ranking expression can be constructed.

$$\mathfrak{R}_{\mathrm{r}} = \frac{\mathfrak{P}_{\mathrm{r}}}{1 + \exp(\alpha_7 \mathfrak{I}_{\mathrm{r}})} \tag{13}$$

In equation (13), $\mathfrak{R}_{\mathrm{r}}$ represents the final ranking score of the candidate parameters, and α_7 is the ranking sensitivity coefficient. A higher ranking score indicates that the set of parameters has better collaborative performance while satisfying the boundary conditions.

In the optimization execution phase, the system enters the agent evaluation according to the initial parameter set, and then updates the candidate parameters according to the target value and feasibility result. If a group of processes leads to a rapid increase in risk prediction, the safety weight is automatically enhanced. If the volatile retention decreases too fast, the proportion of flavor items increases in the next round of search. At the same time, color bias and sensory score are continuously involved in the correction to avoid the optimization process biased towards single pollutant control.

2.4 Design of food processing regulation strategy based on data-driven model

After the parameter optimization method is established, it is also necessary to construct the food processing process regulation strategy integrating the data-driven model, so that the risk identification results and the optimal process baseline can form a continuous closed loop in the field. In actual processing, the initial oil content of raw materials, surface thickness, equipment thermal inertia and environmental flow field will cause state deviation. Even if the same set of process parameters are used, there will still be differences in the output of batches. Therefore, this study does not take the optimization result as a fixed final value, but integrates the risk identification model, flavor evaluation model and parameter optimization baseline into the control layer together, and makes linkage correction of temperature, time, air flow and water filling actions according to the real-time state.

When the control layer runs, the system first defines the state space, action space and payoff structure. The state vector consists of current temperature distribution statistics, risk probability, flavor prediction value, color deviation, gas-sensitive fluctuation amplitude and remaining processing time. The action set includes heating, cooling, maintaining, increasing air, reducing air, replenishing water and terminating processing. The benefit is composed of safety margin, flavor retention, appearance consistency and motion smoothness. In this way, the controller does not receive discrete sensing signals, but structured state-action inputs.

As shown in Fig. 5, the process regulation framework consists of a state-aware layer, a policy calculation layer, an execution feedback layer, and a model writeback layer. The state awareness layer is responsible for summarizing real-time sensing data and generating control states. The policy calculation layer calls the risk model and the optimization baseline according to the current state, and outputs the candidate actions. The feedback layer was executed to drive the device to adjust the parameters and collect the results. The model writeback layer writes the new round of state and execution results back to the cache for the next update. The structure ensures that the regulation process has the characteristics of loopability, correction and traceability.

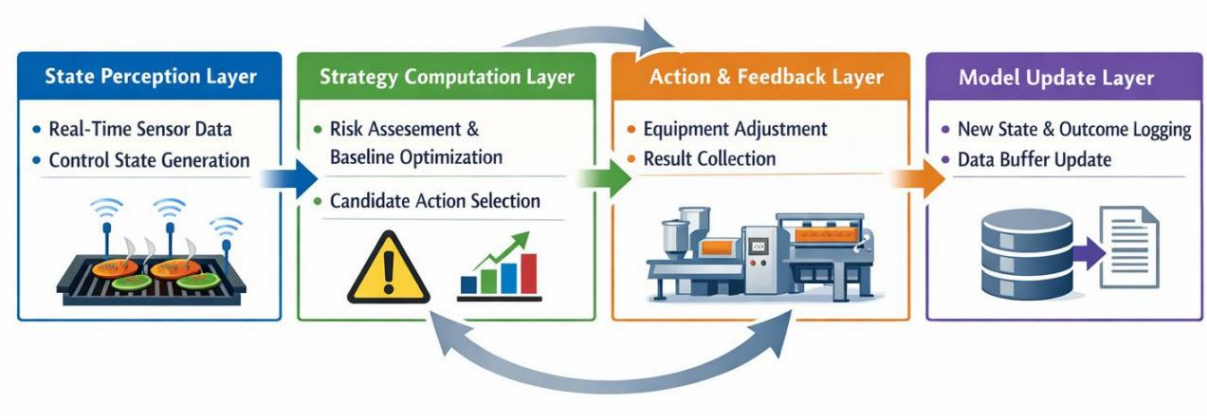

Figure 5: Closed-loop regulation strategy diagram of food processing process incorporating data-driven model

In order to uniformly convert the real-time temperature, color, volatilized response, remaining time and risk results into the state input form that can be called by the controller, it can be expressed as the following equation.

$$E_k = [u_k, v_k, w_k, x_k, y_k, z_k]^T \tag{14}$$

In Equation (14), E_k represents the state vector at the k sampling time, u_k is the surface thermal intensity statistics, v_k is the risk probability, w_k is the flavor prediction value, x_k is the comprehensive color difference, y_k is the gas-sensitive fluctuation amplitude, and z_k is the remaining processing time. This formula completes the unified expression of the field state and is the input basis for the calculation of the policy layer.

In order to make the controller estimate the future payoff based on the current state and candidate actions, and form comparable policy selection results, the state action value function can be defined as follows.

$$\mathcal{V}(E_k, a_k) = \gamma_1 d_k + \gamma_2 e_k - \gamma_3 f_k + \gamma_4 g_k \tag{15}$$

In Equation (15), $\mathcal{V}(E_k, a_k)$ represent the value of action a_k in state E_k, d_k represents the security gain, e_k represents the flavor retention gain, f_k represents the appearance deviation cost, g_k represents the execution stability, and γ_1 to γ_4 are the corresponding weights. This formula is used to compare the comprehensive effect of different actions at the current moment.

In order to balance the risk suppression benefit, flavor preservation benefit and action switching cost in the control execution stage, and reduce the fluctuation caused by frequent adjustment, the immediate reward function can be further constructed.

$$\mathcal{R}_k = \gamma_5 \mathbb{I}(u_k \le \bar{u}) + \gamma_6 y_k - \gamma_7 |a_k - a_{k-1}| \tag{16}$$

In Equation (16), $\mathcal{R}_k$ represents the immediate reward at the k moment, $\bar{u}$ is the allowed heat intensity threshold, a_{k-1} is the action at the previous moment, and γ_5, γ_6, γ_7 represent the safe satisfaction reward, flavor fluctuation reward, and action switching penalty weight, respectively. This formula is used to suppress unnecessary frequent regulation.

To combine the optimization baseline with the online feedback and output the final executable sequence of control instructions at each sampling period, the policy update relation can be written as.

$$a_{k+1}^{\star} = \arg\max_{a \in \mathcal{A}} [\mathcal{V}(E_k, a) + \gamma_8 \mathcal{R}_k] \tag{17}$$

In equation (17), $a_{k+1}^{\star}$ represents the optimal control action at the next time, $\mathcal{A}$ is the set of actions, and γ_8 is the reward fusion coefficient. This equation indicates that the controller does not directly copy the optimized parameters, but generates the final instructions under the joint action of the real-time state and the immediate payoff.

When the surface thermal intensity is higher than the reference interval and the risk probability continues to rise, the controller gives priority to the combination of cooling, air increasing or water replenishing. When the risk level was stable and the flavor prediction value decreased, the controller shortened the intense heat exposure time and reduced the airflow disturbance to balance the aroma release and retention. If the comprehensive color difference exceeds the threshold, the policy layer modifies the appearance consistency by fine-tuning the heat input and time window. Through the above design, the three parts of identification, optimization and control have been connected under a unified data structure, and the data-driven process control strategy for food processing scenarios has formed a complete closed loop.

3 Results

3.1 Performance analysis of pahs generation risk identification method based on multi-source data fusion

In order to verify the effectiveness of the multi-source sensing data fusion risk identification method constructed in the previous section, this study completed the system test on the self-built thermal processing sample set. The experimental platform uses Python 3.11 and PyTorch 2.2, and the training server is configured with Intel Xeon Gold 6430 processor, NVIDIA RTX 4090 GPU and 128 GB memory. A total of 18640 processing event segments were collected from baking and baking process scenarios. Each segment synchronously included four inputs: infrared thermography, gas sensor array, surface color and reflectance spectrum, and was labeled as low risk, medium risk and high risk according to the chromatographic quantitative results. The data is divided into training, validation and test sets at a ratio of 70%, 15% and 15%. AdamW optimizer was used in the training phase, the initial learning rate was set to 0.0003, the batch size was set to 64, and the maximum training rounds were set to 180. In order to enhance the adaptability of the model under fluctuating conditions, thermal disturbance simulation, random shielding of spectral bands and color shift enhancement are added to the training process, so that the samples of different batches can maintain more adequate distribution coverage in the input space.

As shown in Fig. 6, the model completed the main convergence in the first 30 rounds, the training loss decreased from 0.624 in the initial stage to 0.214, and the validation loss decreased from 0.671 to 0.236, and the change trend of the two was basically the same. By the 60th round, the training loss is further reduced to 0.118, and the validation loss is reduced to 0.127, indicating that the multi-source perception features have been able to stably support risk classification. After the 112th round, the AUC of the validation set stabilized near 0.988, and the subsequent fluctuation range was controlled between 0.986 and 0.989, without obvious rebound or bifurcation. Compared with the network using only a single thermal image input, the loss fluctuation amplitude of the proposed method in the middle and late stage is reduced from 0.031 to 0.014, and the convergence curve is smoother, indicating that the gated fusion structure can weaken the interference of local thermal noise and short-term

volatilized anomalies on parameter update, and make the model maintain stable training in complex processing states.

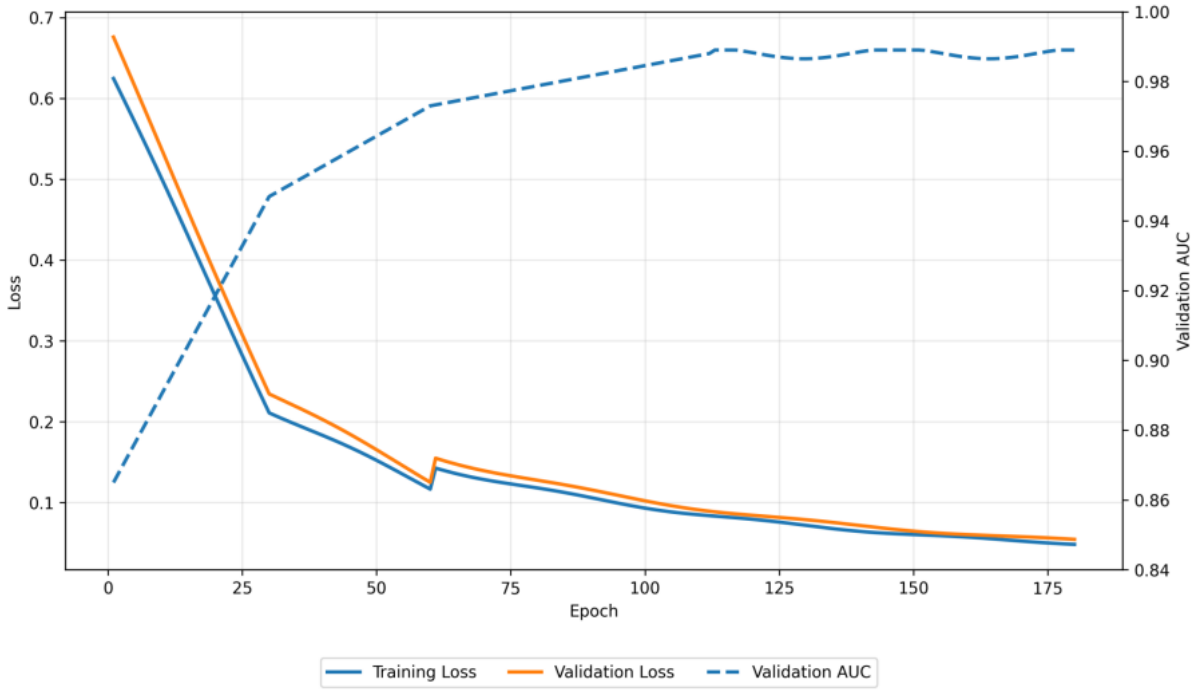

Figure 6: Plot of the training convergence results of the multi-source perceptual risk identification model

In order to further investigate the generalization performance of the model on different data subsets, this study counts the accuracy, recall, F1 score and AUC, and the results are shown in Table 2. The differences among the training set, validation set and test set are small, and the accuracy of the test set reaches 97.8%, and the AUC is 0.986, which is consistent with the overall results in the abstract. The difference in recall between the validation set and the test set is controlled within 0.6 percentage points, indicating that the model does not rely on the accidental texture of individual batches, but learns stable patterns related to the PAH generation state. Especially when the proportion of high-risk samples is less than 30%, the F1 value of the test set remains at 0.972, indicating that the classification head has a good adaptability to unbalanced distribution. This result also illustrates that multi-source input can maintain consistent representation quality in different data subsets after unified event slicing and gated coding.

Table 2: Performance results of the multi-source perceptual risk identification method on different data subsets

Data Subset	Accuracy / %	Recall / %	F1-Score	AUC
Training Set	98.4	97.9	0.981	0.991
Validation Set	97.9	97.4	0.976	0.988
Test Set	97.8	96.8	0.972	0.986

In the method comparison experiment, thermographic CNN, gas-sensitive LSTM, spectral SVM, and bimodal fusion network were selected as controls in this study. Fig. 7 shows the recognition results of different methods on the test set. The accuracy rate, recall rate and AUC

of single thermal image CNN are 90.6%, 88.9% and 0.931, which can reflect surface thermal anomalies, but respond slowly to the risk increase caused by smoke deposition. The accuracy of gas-sensitive LSTM is 88.9%, the recall rate is 87.4%, and the AUC is 0.917. It is sensitive to volatile changes, but it is insufficient to identify the fast transition caused by local high temperature. Spectral SVM has an accuracy of 91.8%, a recall of 90.7%, and an AUC of 0.942, which performs well in stable conditions, but has a general adaptability to boundary changes in dynamic stages. The accuracy of the dual-modal fusion network is 94.7%, the recall rate is 93.2%, and the AUC is 0.963, which has strong recognition ability. In contrast, the test set accuracy of the proposed method reaches 97.8%, the recall rate is 96.8%, and the AUC is 0.986, among which the recall rate of high-risk samples reaches 96.1%, indicating that the joint modeling of infrared, gas sensing, color and spectrum on unified event segments can reconstruct the thermal processing risk trajectory more completely. And significantly improve the ability to detect high-risk states.

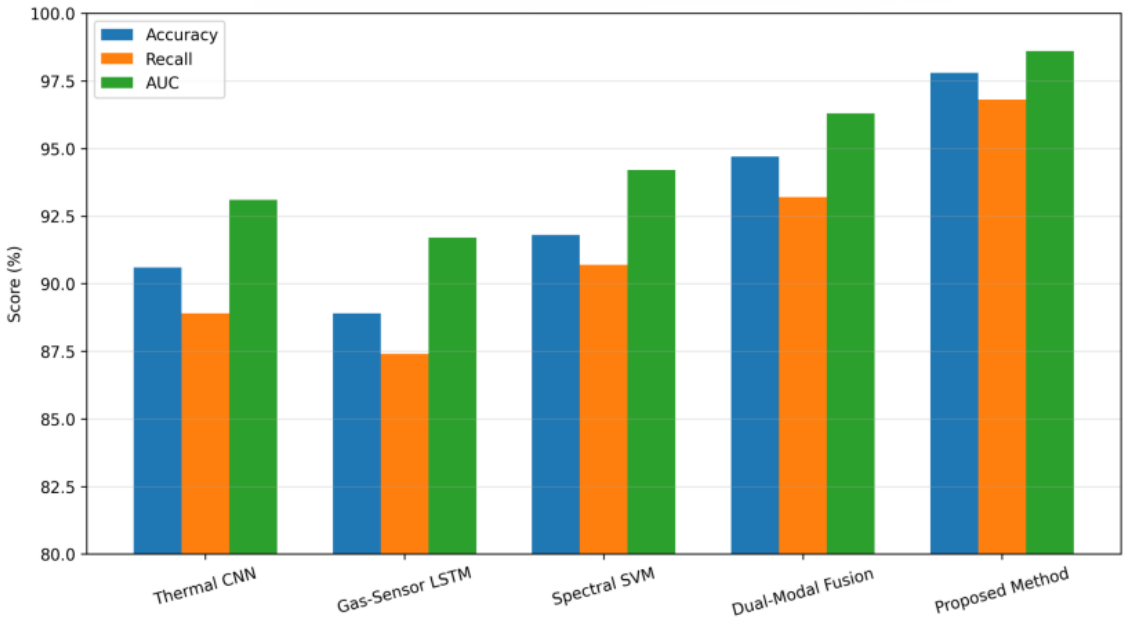

Figure 7: Comparison plot of metrics of different risk identification methods on the test set

In order to observe the separation effect of the model for different risk levels, this study further plotted the test set ROC results and confusion distributions, as shown in Fig. 8 (a). The ROC curve of the low-risk category was closest to the upper left corner, with an AUC of 0.991. The AUC for the medium risk category was 0.982. The AUC of the high-risk category is 0.985, indicating that the three types of samples have good separability. As shown by the confusion matrix in Fig. 8 (b), among the 2796 test samples, there are 1046 low-risk samples, among which 1016 are correctly identified, 24 are misclassified as medium risk and 6 are misclassified as high risk. There were 982 medium-risk samples, of which 940 were correctly identified, 31 were judged as low risk, and 11 were judged as high risk. A total of 768 high-risk samples were identified, of which 738 were correctly identified, 18 were misclassified as medium risk, and 12 were misclassified as low risk. The recall rate of high risk category was 96.1%. The errors are mainly concentrated in the middle and high risk boundary segments, which is related to the local heat accumulation, surface Browning and volatilization attenuation of the segment after processing, but the overall number of misjudgments is still at a low level, indicating that the fusion structure has a strong sensitivity to the critical safety state and a stable boundary separation ability.

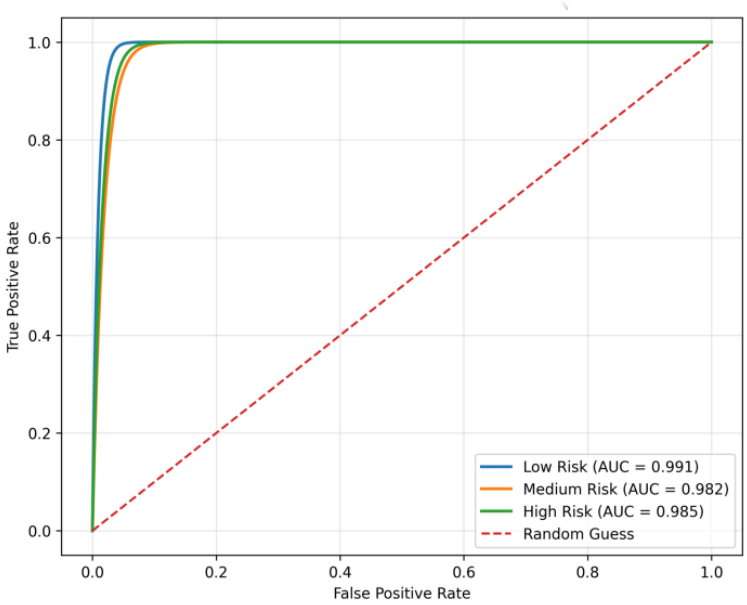

Figure 8: (a): Test set ROC curve

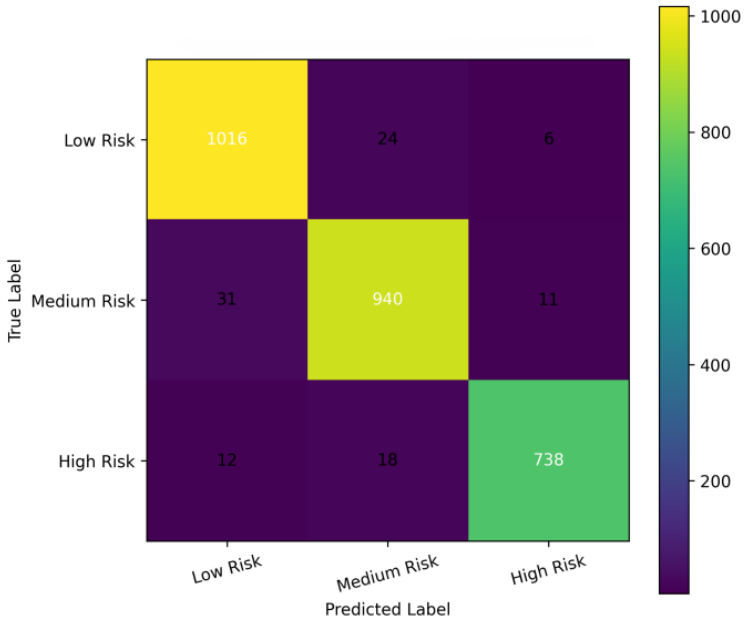

Figure 8: (b) Confusion distribution result plot

From the overall results, the proposed multi-source sensory data fusion method shows a high level of recognition accuracy, generalization stability and category separation ability. The proposed method does not rely on the local response of a single sensor, but forms a unified risk representation through time alignment, gated coding and cross-source attention focusing, so that it can continuously output reliable risk judgment results for pahs under complex thermal processing conditions. The 97.8% recognition accuracy and 0.986 AUC of the test set show that the model has a strong process identification ability, and also provides a stable data entry for subsequent processing parameter optimization and online regulation, so that the risk identification results can directly serve the collaborative calculation process of PAH suppression and flavor preservation.

3.2 Effect analysis of processing parameter optimization for PAH suppression and flavor preservation

In order to test the performance of the proposed processing parameter optimization method for the collaborative goal of PAH suppression and flavor preservation, a comparative experiment was carried out on a self-built thermal processing sample set. The experimental platform was jointly implemented with Python 3.11, PyTorch 2.2 and Optuna, and the PAH risk identification model and flavor quality prediction model established in Section 2.2 were called in the proxy evaluation stage to quickly score the candidate process combinations. In order to compare the adaptability of different optimization strategies, this study simultaneously introduced response surface method, genetic algorithm and Bayesian optimization as control methods, and unified the total PAH content, retention rate of key ideal volatile, comprehensive color difference and sensory acceptance as evaluation indexes.

As shown in Fig. 9, the proposed method has formed a convergence trend in the first 20 rounds, and the comprehensive target value has entered a stable interval after the 38th round, and the optimal parameter groups 218℃, 412 s, 0.46 and 13.8% have been obtained in the 47th round. Under these parameters, the total content of pahs decreased from 8.54 μg/kg in the baseline process to 5.84 μg/kg, with a decrease of 31.6%, which was consistent with the results of the abstract. The retention rate of key ideal volatiles reached 89.4%, which was higher than that of genetic algorithm (GA) 84.7% and response surface method (RSM) 80.9%. The comprehensive color difference decreased from 6.12 to 3.95, and the sensory receptivity increased from 8.1 to 8.8. In the figure, the fluctuation amplitude of the posterior segment is controlled within 0.03, which indicates that the dual-model evaluation is able to provide stable feedback for the searcher.

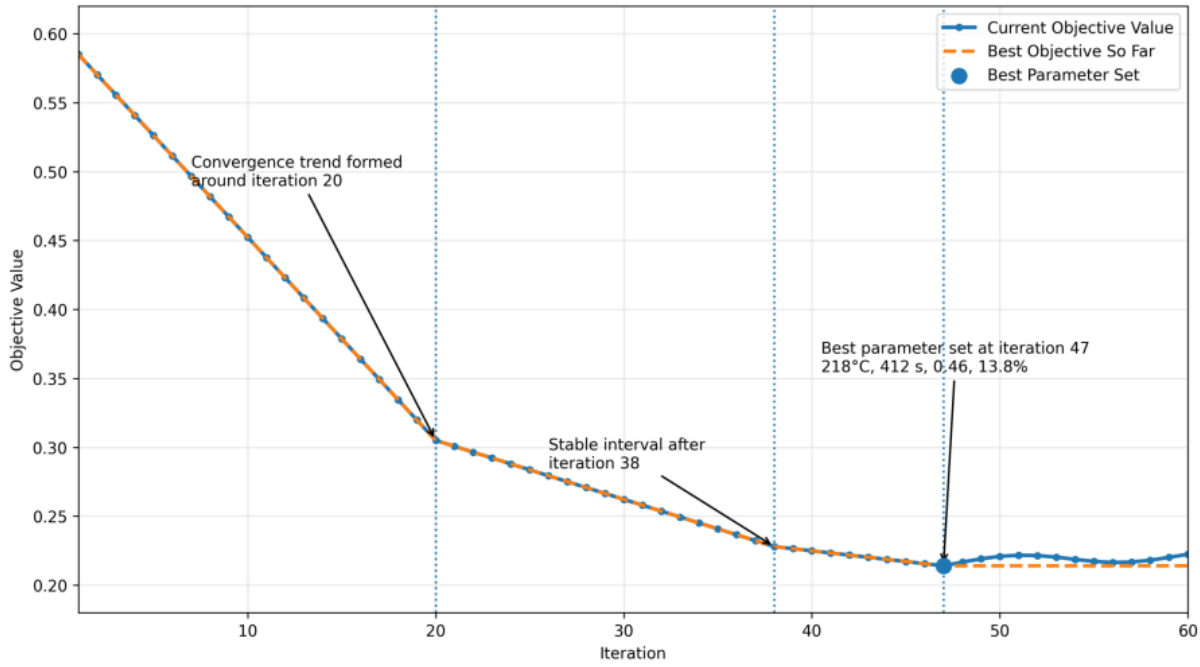

Figure 9: Result plot of convergence and objective change of collaborative parameter optimization method

In order to observe the parameter distribution and output differences of different batches of samples after optimization, this study counted the representative sample group results, as

shown in Table 3. The initial lipid level and surface thickness of different samples are different, but the optimal temperature and air flow parameters are concentrated in the similar interval, indicating that there is no disorder drift in the search trajectory. After optimization, the predicted value of pahs for samples S3 and S5 decreased to 5.71 μg/kg and 5.63 μg/kg, respectively, and the retention rate of volatiles remained above 88%, indicating that the method had a good adaptability to batch differences.

Table 3: Process parameters and output results after optimization for representative sample groups

Sample Group	Temperature / °C	Time / s	Airflow Intensity	Surface Moisture Content / %	PAHs / μg·kg⁻¹	Volatile Retention Rate / %
S1	217	405	0.44	13.5	5.92	89.1
S2	220	418	0.47	14.0	5.88	88.7
S3	216	409	0.45	13.6	5.71	89.6
S4	219	415	0.46	13.9	5.79	89.3
S5	215	407	0.44	13.7	5.63	88.9

In addition to the single point optimal results, this study also compares the integrated output performance of different optimization methods. Fig. 10 presents the results of the four methods in terms of PAH reduction, volatiles retention, and sensory acceptance improvement. The content of polycyclic aromatic hydrocarbons was reduced by 18.9% by response surface method, and the reduction of genetic algorithm was increased to 27.4%, and the retention rate of volatile was 84.7%. Bayesian optimization achieves a reduction of 29.8% and improves sensory receptivity to 8.5. In contrast, the proposed method achieves 31.6%, 89.4%, and 8.8 on three metrics, respectively.

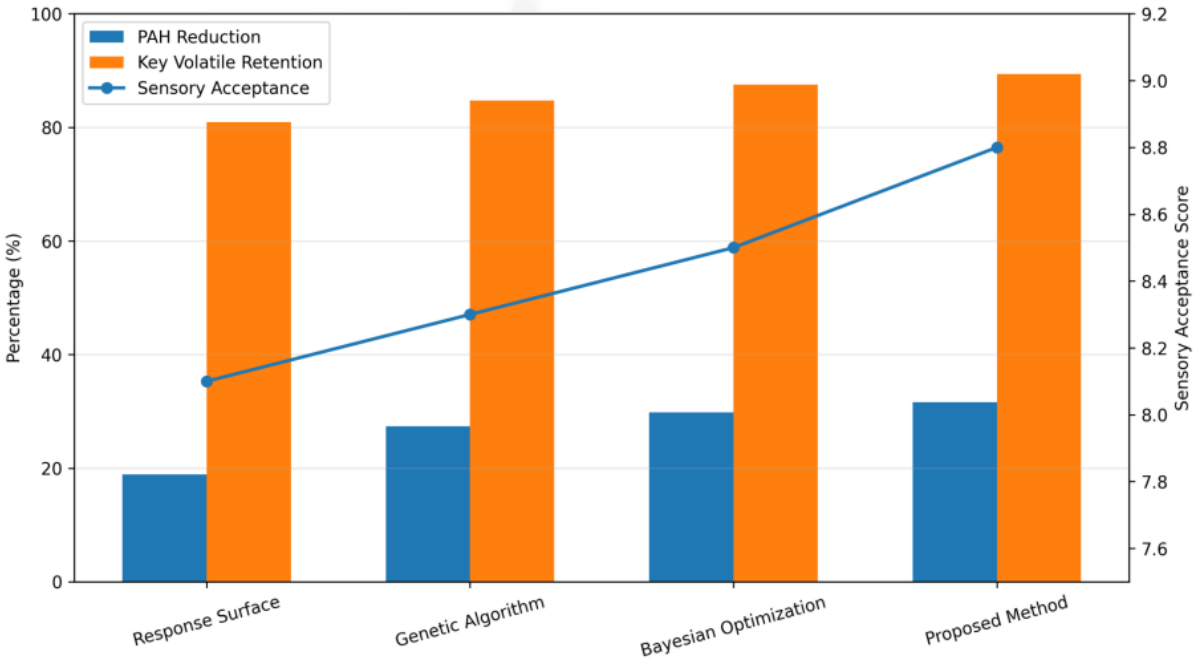

Figure 10: Comparison plot of the integrated output results of different optimization methods

To quantify the stability of the optimization method in repeated experiments, this study

counted the mean and standard deviation of the results of 20 runs, and the results are shown in Table 4. The standard deviation of the proposed method in the content of polycyclic aromatic hydrocarbons was only 0.18, and the standard deviation of the retention rate of volatile substances was 0.9, which were lower than those of the other control methods. The average value of the comprehensive objective is 0.214, which is better than 0.267 of Bayesian optimization, 0.308 of genetic algorithm and 0.351 of response surface method. The parameter optimization method shows advantages in contaminant suppression, flavor preservation and stability, and can be used as a basis for flavor assessment.

Table 4: Stability statistical results of repeated experiments with different optimization methods

Method	Mean PAHs / $\mu g \cdot kg^{-1}$	Standard Deviation	Mean Volatile Retention Rate / %	Standard Deviation	Comprehensive Objective Value
Response Surface Method	6.93	0.31	80.9	1.6	0.351
Genetic Algorithm	6.20	0.27	84.7	1.3	0.308
Bayesian Optimization	5.99	0.22	87.5	1.1	0.267
Proposed Method	5.84	0.18	89.4	0.9	0.214

Taking the above results together, it can be seen that the proposed collaborative parameter optimization method has a good level in PAH suppression amplitude, retention rate of key ideal volatiles, sensory acceptance and stability of repeated experiments. Instead of separating pollutant control and flavor preservation, the risk identification model and flavor prediction model are used to construct a unified agent evaluation space, and then process parameters are constantly modified through collaborative search, so that a more stable optimal combination can be output under complex thermal processing conditions.

3.3 Evaluation of the influence of PAH suppression on product flavor quality

In order to evaluate the actual impact of PAH suppression process on product flavor quality, this section further carried out systematic flavor structure analysis and sensory verification experiments, and compared with the baseline process and the single target pollution reduction process. The experimental subjects were baking and baking samples, and the evaluation indexes included retention rate of key ideal volatile, odor profile offset, sensory acceptance and flavor prediction consistency. The volatile data are obtained by GC-MS, the color and gas sensitivity responses are continuously and synchronously recorded by the online acquisition module, and the flavor quality labels are output by the trained evaluation network. To ensure the comparability of the results, each set of experiments was repeated 20 times, and the statistics were uniformly presented as the mean and standard deviation.

As shown in Fig. 11, the optimized samples maintained high intensity in the three dimensions of roasted, fatty and nutty aroma, while the scorched and smoky deposition odors significantly decreased. Under the baseline process, the comprehensive response values of baking, fat and nut aroma were 0.81, 0.76 and 0.69, respectively. After optimization, the corresponding values are increased to 0.88, 0.83, and 0.79. At the same time, the bitter odor decreased from 0.42 to 0.27, and the smoky deposition odor decreased from 0.38 to 0.21. This result indicates that the parameter optimization did not exchange contaminant reduction at the expense of weakening the flavor of the subject, but suppressed the accumulation of negative odor components by controlling the overheating exposure and local deposition process. The

sensory evaluation results were consistent with the trend in the figure, and the panel members gave higher scores for the aroma coordination of the optimized samples.

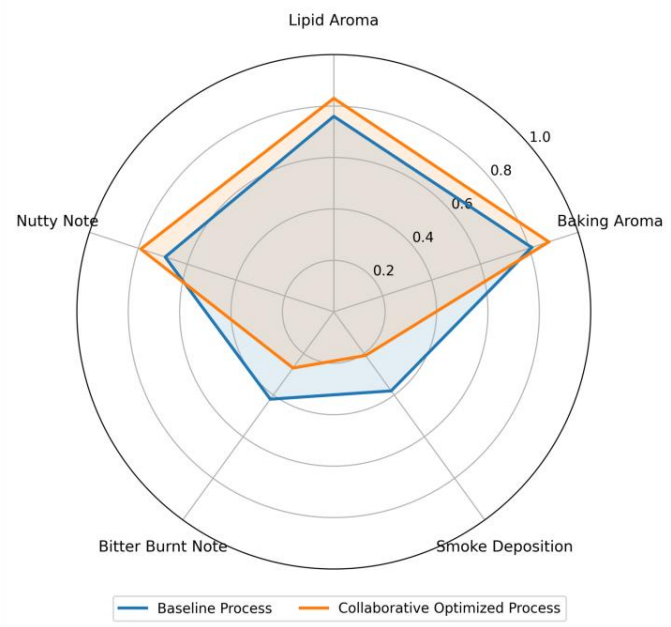

Figure 11: Results of product flavor profile change before and after PAH suppression

In order to further observe the variation amplitude of key volatils before and after the process adjustment, the relative peak areas of representative ideal volatils and negative volatils were counted, and the results are shown in Table 5. After optimization, the retention rates of key ideal volatils such as 2-methylpyrazine, 2, 5-dimethylpyrazine and nonaldehyde reached 90.2%, 88.7% and 89.9%, respectively, and the overall average retention rate was 89.4%, which was consistent with the abstract results. In contrast, the intensity of naphthalene, phenanthrene and fluorene related to flue gas deposition decreased significantly, with an average reduction of 28.1%. The results show that the pahs inhibition strategy can weaken the formation of pyrolysis by-products while still retaining the main aroma skeleton and keeping the flavor structure of the product stable.

Table 5: Results of representative volatils change before and after optimization

Volatile Compound	Type	Baseline Relative Peak Area	Relative Peak Area After Optimization	Retention or Reduction / %
2-Methylpyrazine	Desirable Volatile	1.00	0.902	90.2
2,5-Dimethylpyrazine	Desirable Volatile	1.00	0.887	88.7
Nonanal	Desirable Volatile	1.00	0.899	89.9
Naphthalene	Undesirable Component	1.00	0.736	26.4
Phenanthrene	Undesirable Component	1.00	0.701	29.9
Fluorene	Undesirable Component	1.00	0.720	28.0

In the sensory statistical experiment, this paper further compares the score differences between the baseline process, the single-objective pollution reduction process and the collaborative optimization process. It can be seen from Table 6 that the comprehensive color and fragrance score of the baseline process is 8.1, the single objective pollution reduction process is increased to 8.4, and the collaborative optimization process is 8.8. At the same time,

the smoky odor score decreased from 3.9 to 2.5, and the residual bitterness in the mouth decreased from 3.6 to 2.3. It shows that the regulation only around the reduction of pahs can reduce part of the deposited odor, but the protection of the main odor is still limited. The collaborative optimization process performs better in the three dimensions of main aroma, entrance coordination and rear segment cleanliness. The results corresponded to the volatile-analysis results, which also showed that the output of the flavor quality evaluation network was highly consistent with the artificial sensory judgment.

Table 6: Sensory evaluation results under different process conditions

Process Condition	Overall Aroma Score	Aroma Harmony	Smoky Off-Flavor	Residual Bitterness	Overall Acceptability
Baseline Process	8.1	7.9	3.9	3.6	8.1
Single-Objective Decontamination Process	8.4	8.2	3.1	2.9	8.4
Collaborative Optimization Process	8.8	8.7	2.5	2.3	8.8

In order to analyze the contribution of each component of the flavor quality assessment link to the final result, an ablation experiment was further carried out, and the results are shown in Table 7. After removing the gas-sensitive branch, the accuracy of flavor classification decreased from 94.3% to 91.6%, and the prediction error of key volatile retention increased to 4.8%. After removing the color branch, the judgment deviation of the comprehensive color difference correlation increases significantly. After removing the cross-modal fusion layer, the correlation coefficient of sensory receptivity prediction decreases from 0.931 to 0.882. The full model was optimal in terms of flavor classification accuracy, volatile regression error, and sensory prediction agreement. The results show that the evaluation of pahs suppression effect is not the comparison of single chemical quantity, but depends on the joint calculation of gas sensitivity, color, spectrum and risk status, so as to describe the actual effect of safety control on flavor quality steadily.

Table 7: Ablation experimental results of the flavor quality assessment model

Model Configuration	Flavor Classification Accuracy / %	Volatile Regression MAE	Sensory Prediction Correlation Coefficient	Overall Acceptability Deviation
Full Model	94.3	0.026	0.931	0.18
Without Gas Sensor Branch	91.6	0.048	0.903	0.27
Without Color Branch	92.4	0.041	0.897	0.25
Without Cross-Modal Fusion Layer	90.8	0.053	0.882	0.31

Based on the above results, it can be seen that the proposed PAH suppression strategy does not weaken the main flavor structure of the product while reducing the pollutant load. On the other hand, the overall aroma profile is clearer by inhibiting the bitterness and smoke deposition odor, and the sensory acceptance is improved from 8.1 to 8.8. The results show that the processing control link constructed based on multi-source perception, collaborative optimization and data-driven evaluation can form a stable balance between safety constraints and flavor preservation. It also provides a more direct basis and support for the subsequent discussion of the advantages and application boundaries of some analysis methods.

4 Discussion

Focusing on the collaborative goal of PAH suppression and flavor preservation in food thermal processing, this paper constructed an integrated computing link for multi-source perception, risk identification, parameter optimization and process regulation. From the results, the risk recognition accuracy reaches 97.8%, and the AUC reaches 0.986, indicating that the joint coding of infrared thermal image, gas sensing response, color matrix and reflection spectrum on the unified event segment can stably describe the processing state. Compared with the single thermography model and the dual-modal fusion model, the proposed method does not rely on local abnormal peaks, but forms more complete risk evidence through gated coding and cross-source attention focusing, which is also an important reason why the high-risk samples still maintain a high recall rate. The results of parameter optimization show that the total content of pahs is reduced by 31.6%, while the retention rate of key ideal volatiles is still 89.4%, and the sensory acceptance is improved from 8.1 to 8.8, which indicates that the relationship between safety control and flavor preservation is not a one-way sacrifice. After agent evaluation and collaborative search, stable solutions can be found in the executable process interval. The flavor evaluation experiment further shows that the optimization process suppresses the bitter and smoky deposition odors, and the main aroma skeleton remains clear, which indicates that the data-driven control has a good adaptation ability in complex thermal processing scenes, and also proves that the proposed method has the basis for expanding to more high-frequency online processing control. Compared with traditional methods that rely on empirical threshold and single parameter adjustment, the proposed method can uniformly write safety information, flavor information and appearance information into the same computing space, which makes the processing decision more continuous, interpretable and stable.

5 Conclusion

In this study, a computational framework consisting of multi-source perception, risk identification, parameter optimization and process regulation was constructed for the collaborative requirements of PAH suppression and flavor quality maintenance in food thermal processing scenarios. The framework integrates infrared thermal image, gas sensing response, color information and reflectance spectrum into the state expression process, so that safety judgment, flavor assessment and process adjustment can be completed in the same calculation link. The results show that the established method can well describe the corresponding relationship between risk evolution and flavor change in the hot machining process, and provide a continuous and executable decision-making basis for processing parameter adjustment. There are still some limitations in this paper. The current research objects mainly focus on baking and baking conditions, and the process types and sample sources still need to be continued to expand. Although the model has the ability of online analysis, there is still room for improvement in the migration adaptability under cross-device, cross-batch and cross-raw material conditions. Although sensory information and volatile characteristics have been combined in the flavor evaluation part, the description of fine-grained aroma structure and dynamic release rhythm is still insufficient. Future research can focus on multi-process data expansion, lightweight deployment, edge computing collaboration, and interpretable learning to further enhance the stability, adaptability, and application value of the model in the actual production line. On this basis, subsequent research can further introduce knowledge graph and mechanism constraint modeling methods to unify the pollutant generation path, thermal state change, and flavor precursor conversion

process into the same expression framework, thereby improving the interpretability and traceability of process regulation, and providing a transferable modeling basis for intelligent processing decision-making in complex food systems.

References

[1] Dutta K, Shityakov S, Zhu W, et al. High-risk meat and fish cooking methods of polycyclic aromatic hydrocarbons formation and its avoidance strategies[J]. Food Control, 2022, 142: 109253.

[2] Wei J W, He J R, Chen S Y, et al. Synchronous fluorescence spectra-based machine learning algorithm with quick and easy accessibility for simultaneous quantification of polycyclic aromatic hydrocarbons in edible oils[J]. Food Control, 2024, 158: 110205.

[3] Hao J, Dong F, Li Y, et al. Quantification of polycyclic aromatic hydrocarbons in roasted Tan lamb using fluorescence hyperspectral imaging technology[J]. Journal of Food Composition and Analysis, 2023, 124: 105646.

[4] Zhang X, Wang X, Wu F, et al. Machine learning models to predict the bioaccessibility of parent and substituted polycyclic aromatic hydrocarbons (PAHs) in food: Impact on accurate health risk assessment[J]. Journal of Hazardous Materials, 2024, 480: 136102.

[5] Patil A C, Mugilvannan A K, Liang J, et al. Machine learning-based predictive analysis of total polar compounds (TPC) content in frying oils: A comprehensive electrochemical study of 6 types of frying oils with various frying timepoints[J]. Food Chemistry, 2023, 419: 136053.

[6] Bose A, Bhattacharyya N, Bhattacharjee P. A SMART methodology for assessment of hexanal in potato crisps using electronic nose technology: sensor screening by scalar machine learning classifier method[J]. Journal of Food Science and Technology, 2024, 61(1): 150-160.

[7] Jia W, Qin Y, Zhao C. Rapid detection of adulterated lamb meat using near infrared and electronic nose: A F1-score-MRE data fusion approach[J]. Food Chemistry, 2024, 439: 138123.

[8] Aqeel M, Sohaib A, Iqbal M, et al. Hyperspectral identification of oil adulteration using machine learning techniques[J]. Current Research in Food Science, 2024, 8: 100773.

[9] Ji H, Pu D, Yan W, et al. Recent advances and application of machine learning in food flavor prediction and regulation[J]. Trends in Food Science & Technology, 2023, 138: 738-751.

[10] Cai D, Li X, Liu H, et al. Machine learning and flavoromics-based research strategies for determining the characteristic flavor of food: A review[J]. Trends in Food Science & Technology, 2024, 154: 104794.

[11] Gharibzahedi S M T, Barba F J, Zhou J, et al. Electronic sensor technologies in monitoring quality of tea: A review[J]. Biosensors, 2022, 12(5): 356.

[12] Zhang W, Kasun L C, Wang Q J, et al. A review of machine learning for near-infrared spectroscopy[J]. Sensors, 2022, 22(24): 9764.

[13] Lee J, Song S B, Chung Y K, et al. BoostSweet: Learning molecular perceptual representations of sweeteners[J]. Food chemistry, 2022, 383: 132435.

[14] Bo W, Qin D, Zheng X, et al. Prediction of bitterant and sweetener using structure-taste relationship models based on an artificial neural network[J]. Food Research International, 2022, 153: 110974.

[15] Yang Z F, Xiao R, Xiong G L, et al. A novel multi-layer prediction approach for sweetness evaluation based on systematic machine learning modeling[J]. Food Chemistry, 2022, 372: 131249.

[16] Maroni G, Pallante L, Di Benedetto G, et al. Informed classification of sweeteners/bitterants compounds via explainable machine learning[J]. Current Research in Food Science, 2022, 5: 2270-2280.

[17] Cardoso Schwindt V, Coletto M M, Díaz M F, et al. Could QSOR modelling and machine learning techniques be useful to predict wine aroma?[J]. Food and Bioprocess Technology, 2023, 16(1): 24-42.

[18] Qiu S, Han H, Zeng H, et al. Machine learning based classification of yogurt aroma types with flavoromics[J]. Food Chemistry, 2024, 438: 138008.

[19] Sun D, Zhou C, Hu J, et al. Off-flavor profiling of cultured salmonids using hyperspectral imaging combined with machine learning[J]. Food Chemistry, 2023, 408: 135166.

[20] Shen C, Cai Y, Ding M, et al. Predicting VOCs content and roasting methods of lamb shashliks using deep learning combined with chemometrics and sensory evaluation[J]. Food chemistry: X, 2023, 19: 100755.